Eur. J. Mineral.
2011, **23**, 343–353
Published online June 2011

This paper was presented at the EMPG XIII symposium in Toulouse, France (April 2010)

REE and Hf distribution between pyrope and NaCl-bearing water at eclogitic-facies conditions

CÉLINE MARTIN[1,2,*], FABRICE BRUNET[3,4], STÉPHANIE DUCHÊNE[1,5], BÉATRICE LUAIS[1] and ETIENNE DELOULE[1]

[1] CRPG, Nancy-Université, CNRS, 15 rue Notre Dame des Pauvres, 54501 Vandoeuvre les Nancy cedex, France
[2] DGLG-WE-Vrije Universiteit Brussel, Pleinlaan 2, 1050 Brussels, Belgium
*Corresponding author, e-mail: celine.martin@vub.ac.be
[3] Laboratoire de Géologie, Ecole normale supérieure, CNRS, 24 rue Lhomond, 75231 Paris cedex 05, France
[4] Institut des Sciences de la Terre, CNRS, Université Joseph Fourier, BP53, 38041 Grenoble cedex 9, France
[5] Laboratoire des Mécanismes de Transferts en Géologie (LMTG), UMR 5563, CNRS – UPS Toulouse III – IRD, 14 rue Edouard Belin, 31400 Toulouse, France

Abstract: Due to the interaction of oceanic crust with seawater, NaCl is a main component dissolved in aqueous fluid in subduction zones. The effect of dissolved NaCl (1.64 mol/l) on the partitioning of REE and Hf between garnet (pyrope) and aqueous fluid (doped with ~500 ppm of REE and ~250 ppm of Hf) has been investigated experimentally at 3 GPa, 850 °C (*i.e.,* eclogitic UH*P* conditions) using the diamond trap technique. Trace elements in both pyrope and diamond aggregate were analyzed using LA-ICP-MS to derive fluid/pyrope partition coefficients (D). Mass balance calculation indicates that lanthanum is present in an accessory phase, törnebohmite. Europium and aluminium concentrations are too high in the aggregate to comply with mass balance and solubility data from the literature, respectively. Transport of these species from the mineral powder to the aggregate is inferred. D_{MREE} (Gd and Tb) equals 0.39 ± 0.11 and 0.22 ± 0.07, respectively. D_{HREE} (Dy to Lu) ranges from 0.09 ± 0.02 to 0.02 ± 0.01 with a regular decrease from Dy to Lu. D_{Hf} is 0.33 ± 0.09. Lanthanum is found to be incompatible (D_{La} is 2.10 ± 0.95) whereas for the other LREE (from Ce to Sm), D is lower than 1 ($D_{Ce} = 0.65 \pm 0.15$, $D_{Pr} = 0.74 \pm 0.22$, $D_{Nd} = 0.71 \pm 0.29$ and $D_{Sm} = 0.61 \pm 0.23$). Contrary to D_{HREE} and D_{MREE}, D_{LREE} do not fit a near-parabolic dependence on LREE effective ionic radius. The Hf fluid/pyrope partition coefficient ($D_{Hf} = 0.33 \pm 0.09$) indicates that this element favourably partition into garnet.

Finally, it is shown that, compared to pure water, the addition of NaCl in water has no significant effect on REE and Hf behaviour.

Key-words: REE and Hf partitioning, pyrope, garnet, törnebohmite, mass balance, mass transport, diamond trap technique.

1. Introduction

Hydrous fluids produced by sediment dehydration in the down-going slab are efficient agents for leaching and transferring trace elements from oceanic crust to the source of arc magmas in the mantle wedge (*e.g.*, Maury *et al*., 1992; Plank & Langmuir, 1993; Tatsumi & Eggins, 1995; Elliot *et al*., 1997; Elliot, 2003). The composition (either major or trace elements) of hydrous fluids produced at depth in subduction zones is not directly measurable but it can be assessed by several indirect means: (1) sampling subduction fluids emanating at the seafloor (*e.g.*, Mottl, 1992; Fryer *et al*., 1997; Silver *et al*., 2000; Hulme *et al*., 2010), (2) analysis of fluid inclusions (*e.g.*, Philippot & Selverstone, 1991; Scambelluri & Philippot, 2001) and metamorphic veins (*e.g.*, Becker *et al.,* 2000; Spandler & Hermann, 2006) from subducted oceanic lithosphere exhumed in collision zones and (3) laboratory experiments under relevant subduction *P-T* conditions (*e.g.*, Brenan *et al*., 1994; You & Gieskes, 2001; Manning, 2004; Feineman *et al*., 2007). Many of these studies point out the importance of chlorine as a main dissolved species (Manning, 2004) related to the interaction between oceanic crust and seawater.

However, solubility and speciation of REE and HFSE (by Cl or other ligands) in natural aqueous fluids can only be modeled for a restricted pressure range, up to *ca.* 500 MPa (*e.g.*, Haas *et al*., 1995). Beyond that *P-T* range, molecular simulation may become an alternative approach through the calculation of the energetics of various REE complexes in aqueous fluids (van Sijl *et al*., 2009).

The composition of the aqueous fluid and, in particular, its Cl content, can influence mineral/fluid partition coefficients through specific speciation (Bau, 1996). For example, chondrite-normalized REE concentration patterns for submarine hydrothermal vent fluids show large positive Eu anomalies (Michard, 1989; Klinkhammer *et al*., 1994; Allen & Seyfried, 2005). Haas *et al.* (1995) were able to

0935-1221/11/0023-2124 $ 4.95
DOI: 10.1127/0935-1221/2011/0023-2124

show on the basis of thermochemical modelling that this Eu anomaly could be related to the strong complexation of Eu^{2+} by aqueous chloride during mineral-rock interactions at high temperatures (*ca.* 300 °C). With respect to the complexing role of Cl in aqueous fluids, Gammons *et al.* (1996) showed, experimentally, a strong and positive temperature effect (in the 25–300 °C range) on the stabilization of Nd chloride complexes.

At higher *P* and *T* (subduction zone conditions), Keppler (1996) showed experimentally that chlorine has a drastic effect on the partition coefficients between minerals and aqueous fluids for LILE, through the complexation of moderately hard acids such as Rb^{+}, Ba^{2+}, Sr^{2+}, Pb^{2+} and K^{+}. The addition of NaCl to H_2O has also been shown to strongly increase the solubility of $CePO_4$ monazite under high grade metamorphic conditions (Tropper *et al*., 2011).

Therefore, based on the recognized role of Cl as a ligand in aqueous fluids, we explore experimentally, here, the effect of NaCl on the REE and Hf behavior in an aqueous fluid under UH*P* eclogitic conditions (3 GPa, 850 °C) as encountered in subduction zones. For that purpose, the partitioning coefficient of these trace elements between NaCl-bearing aqueous fluid and pyrope garnet, $Mg_3Al_2(SiO_4)_3$, were retrieved using the diamond-trap technique and compared to the corresponding partition coefficient in ''pure'' water. Pyrope was chosen because garnet is one of main host for trace elements in eclogites (especially HREE and Hf). Furthermore, garnet is used as geochronometer since REE/HFSE can be highly fractionated in this mineral (Lu/Hf ratio up to 8, Duchêne *et al*., 1997). The use of a single solid phase in mineral/fluid partitioning experiments allows complementary mass balance calculations to be performed to double check the analytical data.

The few experiments performed on REE behavior in aqueous fluids at high pressures and temperatures, either conducted with initially pure water and whole rocks (Mysen, 1979; Ayers *et al*., 1997; Kessel *et al*., 2005) or with pure water and a single mineral phase (*e.g.* Brenan, 1993; Brenan *et al*., 1995; Stalder *et al*., 1998) indicate that LREE are more favorably partitioned into aqueous fluids than HREE. Moreover, Stalder *et al*. (1998) have shown that the presence of chlorine anions (HCl) has no significant effect on the partitioning of some of these trace elements.

2. Experimental techniques

2.1. Starting materials and experimental strategy

A solid starting material with a $H_3MgO : Al_2O_3 : 3SiO_2$ pyrope composition was obtained from a TEOS gel (tetraethylorthosilicate) using $Mg(NO_3)_2$ and $Al(NO_3)_3$ as magnesium and aluminium sources, respectively (see Brunet & Chazot, 2001 for more details). A 0.05 N HNO_3 aqueous solution doped with 500 ppm of each of the REE and *ca.* 250 ppm of Hf was prepared from a REE Accutrace standard solution and a Hf Accutrace standard solution. In the following, REE and Hf will be referred to as *trace elements.* Ninety-six grams of NaCl were added to part of this trace element-doped solution in order to test the effect of dissolved sodium chloride on mineral/fluid trace elements partitioning.

HREE are expected to preferentially partition into garnet (Harrison & Wood, 1980), therefore, concomitantly to the garnet crystallization from the starting gel, the H*P*-H*T* solution will progressively become depleted with respect to HREE. Consequently, a bell-shaped zoning in HREE is expected in garnet (Hollister, 1966), especially given the high garnet/solution mass ratios (2.75) used in this study. In order to limit intragranular heterogeneity as well as to constrain homogeneization timescale, a two-step process of garnet synthesis and fluid/mineral equilibration has been followed. All experiments were carried out at 850 °C and 3 GPa in a piston-cylinder apparatus using NaCl-based low-friction cells (1/2'') at ENS (Paris). Synthetic garnets were first crystallized from 133.3 mg of solid starting material in the presence of the doped solution (48.3 µl of NaCl-solution), for 24 h, in an Au-capsule of 4.4 mm inner diameter (4.8 mm outer diameter) welded shut. These experiments were designed to achieve a first step towards trace elements equilibration. This first equilibration step will be called Step 1 or S1 hereafter. The run product is then crushed in an agate mortar down to a maximal grain size of 1 micron. Then, 47.7 mg of it are loaded in an Au-capsule (2 mm outer diameter) and run a second time (Step 2) for 6 days with the NaCl-bearing aqueous solution (10.9 µl). This experiment will be called S2. The experimental load (Fig. 1) was made of two layers of synthetic pyrope, and an intermediate 1 mm-thick layer of polycrystalline synthetic diamond (grains of 8–15 µm in

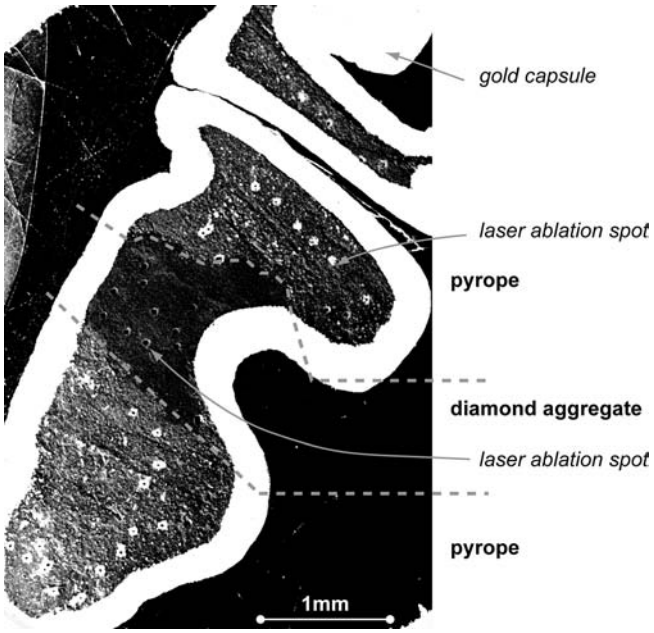

Fig. 1. SEM image of the whole charge showing the pyrope – diamond aggregate – pyrope sandwich and laser ablation spots.

diameter) used to trap the matter dissolved in the H*P*-H*T* fluid upon quenching (*e.g.*, Stalder *et al*., 1998; Kessel *et al*., 2005).

2.2. Synthesis detail and analytical techniques

After the end of the S1 experiments, the capsule is carefully cleaned with alcohol and distillated water, then it is opened and both solution and garnet crystals are poured in a Teflon beaker. The inner capsule is rinsed with deionized water (18.2 Ω) which is collected in the same beaker. Both the solid fraction and fluid are centrifuged, then the fluid is recovered with a syringe and the solid fraction is X-rayed. The residual solution is analyzed for major and trace elements (Table 1) by ICP-AES and ICP–MS respectively (SARM, CRPG-CNRS, Nancy). Some grains are mounted in epoxy for further analyses (EMP, LA-ICPMS).

After quenching of the S2 experiment, capsule is weighed and pierced in a Teflon beaker which is then closed and put on a hotplate (90 °C) for 2 h. The fluid collected by evaporation is sampled for further chemical analyses (Table 1). After this drying process, the capsule is weighed again and mounted in epoxy. Only ethanol was used to clean mount and polish the sample in order to avoid re-dissolution of material trapped within the porosity of the diamond aggregate.

X-ray powder diffraction was performed with a Rigaku UltraX18HF (Cu rotating anode) in a Bragg – Brentano geometry (ENS, Paris). Major elements analyses of the solid fraction was performed with a Cameca-SX100 electron microprobe (Service commun de microscopies électroniques et microanalyses X, UHP, Nancy) with an acceleration voltage of 15 kV, a beam current of 10 nA and a counting time of 20 s except for Na (10 s) both in pyrope and diamond aggregates. La, Nd, Yb, Lu and Hf have also been analyzed using the electron microprobe (acceleration voltage of 25 kV, beam current of 100 nA and a counting time of 240 s for Yb, Lu and Hf and 120 s for La and Nd) with 1 σ precision <0.03% for Yb, Lu and Hf and <0.01 % for La and Nd concentrations. Images of the diamond aggregate and garnet were collected using a FE-SEM (Service commun de microscopies électroniques et microanalyses X, UHP, Nancy) with an acceleration voltage of 20 kV and a beam current of 5 nA. Semi-quantitative analyses of accessory phases are performed by EDS with both FE-SEM and TEM.

The trace element content of both pyrope garnet (Step 1 and 2) and solid residue trapped in the diamond aggregate (Step 2) were analyzed by LA-ICP-MS using a 800 nm (60 fs) laser coupled with a ICP-MS Agilent 7500Ce (LMTG, Toulouse). The laser beam is of ∼25–30 μm in diameter. We analyzed for ^{27}Al, ^{29}Si, ^{45}Sc, ^{139}La, ^{140}Ce, ^{141}Pr, ^{146}Nd, ^{147}Sm, ^{153}Eu, ^{157}Gd, ^{159}Tb, ^{163}Dy, ^{165}Ho, ^{166}Er, ^{169}Tm, ^{172}Yb, ^{175}Lu, ^{178}Hf, ^{179}Hf (Table 2). In order to monitor LA-ICP-MS analyses, standard NIST 610 was run

Table 1. Major and trace elements in the residuals fluids (in ppm).

	S1	*S2
Si	0.00	33.46
Al	0.00	0.00
Mg	0.00	0.00
Na	30,826.83	2760.15
La	4.99	0.20
Ce	0.18	0.10
Pr	2.53	0.14
Nd	2.02	0.13
Sm	0.78	0.11
Eu	0.48	0.14
Gd	0.21	0.11
Tb	0.17	0.08
Dy	0.16	0.07
Ho	0.13	0.07
Er	0.13	0.07
Tm	0.13	0.07
Yb	0.13	0.07
Lu	0.13	0.07
Hf	0.11	0.02

*Collected by evaporation (Step 2).

Table 2. Analytical conditions for the LA-ICP-MS analyses.

ICP-MS		LA	Custom system
Forward power	1550 W	Wavelengh	800 nm
Gas flows		Repetition Rate	5Hz
Plasma (Ar)	15 l/min	Pulse duration	60 fs
Auxiliary (Ar)	0.9 l/min	Focusing objective	15X, f.l.=13 mm
Carrier (He)	0.46 l/min	Spot size	26 μm
Make-up (Ar)	1.14 l/min	Incident pulse energy	85 μJ/pulse
Shield Torch	Used for all analyses		

Data acquisition parameters	
Data acquisition protocol	Time-resolved analysis
Scanning Mode	Peak hopping, 1 point per peak
Detector mode	Pulse counting, dead-time correction applied
Isotopes determined	^{27}Al, ^{29}Si, ^{45}Sc, ^{139}La, ^{140}Ce, ^{141}Pr, ^{146}Nd, ^{147}Sm, ^{153}Eu, ^{157}Gd, ^{159}Tb, ^{163}Dy, ^{165}Ho, ^{166}Er, ^{169}Tm, ^{172}Yb, ^{175}Lu, ^{178}Hf, ^{179}Hf
Dwell Time	25 ms
Quadrupole settling time	*ca*. 5 ms

systematically two times before and after each five analyses. Aluminium content measured beforehand using the electron microprobe under defocused beam was used to normalize the trace element concentration in pyrope and in the diamond aggregate.

3. Results

3.1. Mineralogy

X-ray diffraction confirms that the run product obtained during S1 is composed of pyrope with minor amounts of Mg-staurolite (Fig. 2). Inspection of the experimental charge using SEM indicates that garnet crystals from experiment S1-NaCl are 50 to 100 μm large with bright cores on BSE images (Fig. 3a). The grain obtained after Step 2 are more homogeneous in size (∼70 μm) and only few bright cores remaining in the S2 experiment (Fig. 3b). Detailed inspection of experimental charges using FE-SEM allows to identify nanocrystals of törnebohmite ($LREE_2Al(OH)[SiO_4]_2$) included in pyrope crystals, by EDS analyses (Table 3, Figs. 4a, b). The small size of these inclusions does not allow to obtain quantitative compositions. Euhedral crystals (*e.g.*, Fig. 4b) with a morphology characteristics of the monoclinic system, present a long side/short side ratio of 1.41, in good agreement with the *a: b* ratio of törnebohmite (*a: b* = 1.3, Shen & Moore, 1982). Törnebohmite was carefully sought in diamond aggregates but was not observed. In S2, euhedral crystals of halite as well as rare corundum grains are spread in the whole experimental charge. They are REE and Hf-free. FE-SEM images of diamond aggregate also display small (100–200 nm) elongated phases containing SiO_2 and/or Al_2O_3 that are assumed to represent quenched material based on the shape and the small size of the grains.

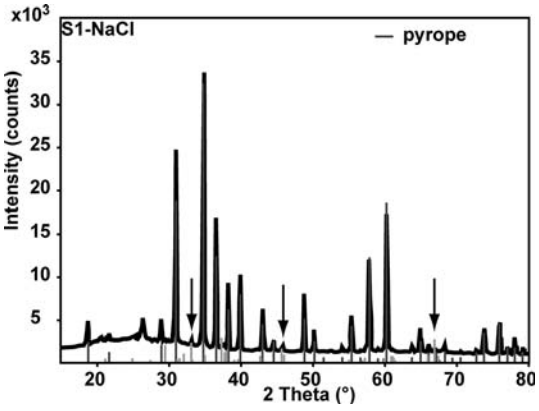

Fig. 2. XRPD pattern obtained on S1 run product. *Arrows* indicate Mg-staurolite reflexions.

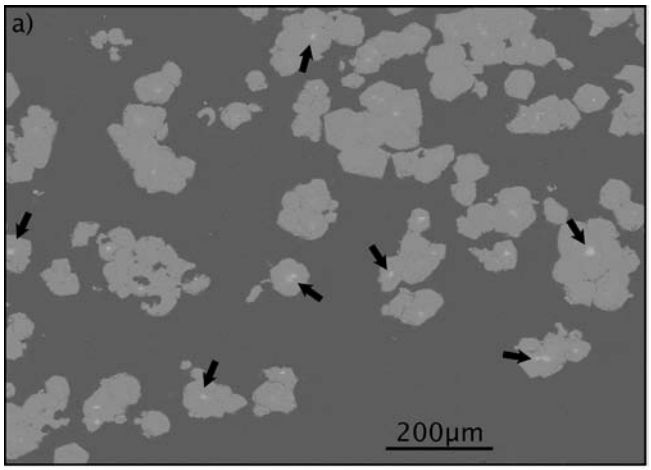

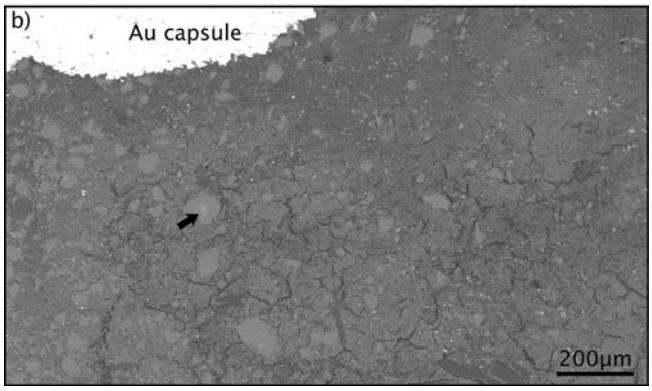

Fig. 3. BSE images of experimental products. (a) S1, (b) S2. Bright cores (HREE rich) are highlighted by *arrows*; their abundance strongly decreases from S1 to S2.

Table 3. Semi-quantitative EDS analyses of törnebohmite partly contaminated by the host pyrope.

	S1	S2
Al_2O_3	*18.40*	*22.98*
SiO_2	*38.95*	*45.52*
MgO	*13.44*	*23.75*
La_2O_3	*23.44*	*2.45*
Ce_2O_3	0.00	0.00
Pr_2O_3	<d. l.	<d. l.
Nd_2O_3	0.52	1.73
Sm_2O_3	<d. l.	<d. l.
Eu_2O_3	<d. l.	<d. l.
Gd_2O_3	<d. l.	<d. l.
Tb_2O_3	<d. l.	<d. l.
Dy_2O_3	<d. l.	<d. l.
Ho_2O_3	<d. l.	<d. l.
Er_2O_3	<d. l.	<d. l.
Tm_2O_3	<d. l.	<d. l.
Yb_2O_3	<d. l.	<d. l.
Lu_2O_3	<d. l.	<d. l.
HfO_2	<d. l.	< d. l.
ThO_2	5.27	2.32
$n^{\#}$	4	2

Notes: values are average values per capsule in wt%; the oxide data the most influenced by the pyrope contamination are in italics.
$n^{\#}$, number of measurements.
<d. l., below detection limit.

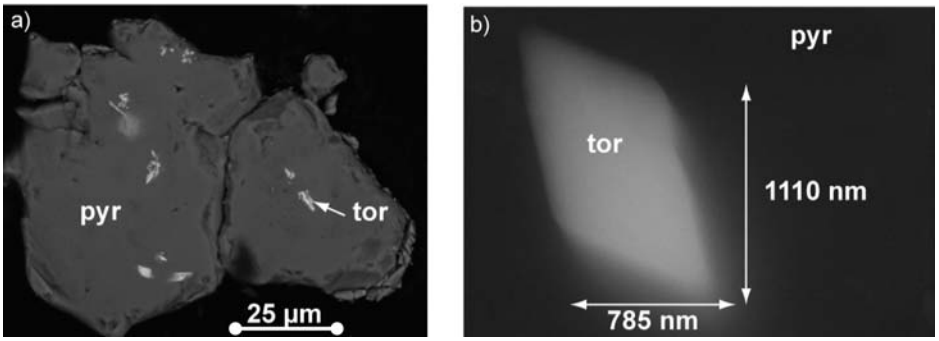

Fig. 4. Microphotograph (BSE mode) of törnebohmite (tor) (a) included in pyrope (pyr) from S1, (b) included in pyrope from S2.

3.2. EMP and LA-ICPMS data

Electron microprobe analyses show that pyrope grains obtained after S1 are zoned in both major and trace elements, with Lu, Yb and Al-rich cores and Mg-rich rims (Fig. 5a). The profiles collected along S2 pyrope grains do not display such contrasted trace element distribution (Table 4 and Fig. 5b).

Since the diameter of the laser spot is large (∼30 µm) compared to the mean pyrope size (50–70 µm across), LA-ICPMS data will partly average out the compositional heterogeneity of the grains. Except La (71 ± 16 ppm) and Ce (471 ± 53 ppm), all the REE concentrations range from 202 ± 55 (Tm) to 328 ± 56 ppm (Eu) and Hf content is 268 ± 47 ppm (Table 4).

The LA-ICPMS data collected on garnet grains from S2 are slightly less scattered. All the average concentrations range from 101 ± 31 ppm (La) to 331 ± 78 ppm (Yb) but they are mainly centered around 200 and 300 ppm. Hf concentration is slightly lower (130 ± 28 ppm) than in S1 and than REE concentrations (Table 4).

In the solid residues trapped in diamond aggregates, REE (excluding Eu) concentrations range from 1 ± 0.3 ppm (Lu) to 53 ± 18 ppm (La) with the highest values encountered for LREE. It should be noted that Eu concentration reaches 312 ± 65 ppm, *i.e.,* six times higher than that of La.

Trace elements concentrations in the residual fluid collected after Step 1 and Step 2 (Table 1) are negligible (four orders of magnitude lower than those of pyrope and diamond aggregates, Table 4). We can therefore assume that the trace elements introduced in the course of S1 and S2 are all partitioned between pyrope and the diamond trap at the end of the experiment (*i.e.,* all the trace elements remained in the capsule after removal of the fluid).

3.3. Calculation of fluid composition

The microdiamond aggregate is an open porous network which is partly filled by solid material. This solid material is expected to represent quench products which have precipitated (1) in the course of the quench stage when *P* and *T* were decreased down to ambient or (2) while the capsule was pierced and the solution evaporated. The solid material trapped within the diamond aggregate could also result from mass transport from the pyrope zone towards the diamond aggregate, due to equilibration with the starting solution (Verlaguet *et al*., 2006; Verlaguet & Brunet, 2007) or due to mass transport along a thermal gradient (Goffé *et al*., 1987). Laser spots are bigger (∼30 µm) than diamond crystal diameter (8–15 µm) and analyses performed in diamonds aggregates (hereafter referred to as *diam*) are assumed to represent a mix from different contributions: the interstitial solid resulting from quench and the diamond crystals. The concentration in the fluid at high pressure (hereafter referred to as fl*H*P) can be calculated from the concentration measured in diamond aggregate using Na as a conservative element.

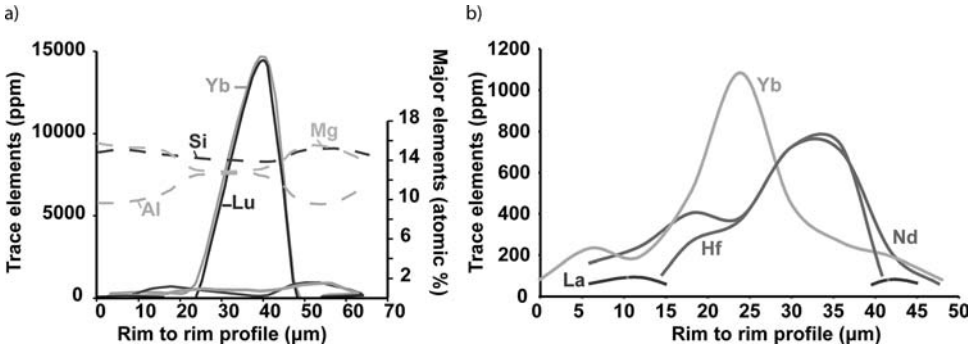

Fig. 5. Major elements and La, Nd, Yb, Lu, Hf rim to rim profiles in pyrope (a) obtained in S1, (b) in S2.

Table 4. Major and trace elements compositions in solid materials. Major elements are in wt% and trace elements in ppm.

Experiment	S1		S2		S2	S2
Material	Pyrope		Pyrope		Diamond aggregate	H*P* fluid
Data obtained by EMP						
	core[¥]	rim[¥]	core[¥]	rim[¥]		#
SiO_2	41.77 ± 0.79	44.43 ± 0.25	44.95	43.38 ± 1.07	4.66 ± 0.99	18.68 ± 3.97
Al_2O_3	25.96 ± 1.49	25.63 ± 0.42	26.95	26.35 ± 1.82	8.25 ± 0.71	33.08 ± 2.86
MgO	27.51 ± 0.74	29.47 ± 0.27	24.66	28.73 ± 0.74	0.19 ± 0.01	0.76 ± 0.04
Na_2O	/	/	/	/	1.61 ± 0.10	6.45 ± 0.40
Total	97.56	99.72	98.18	98.93	14.75	
N	4	15	1	10	6	
La	<d. l.	65 ± 18	<d. l.	120 ± 5		
Nd	108 ± 29	304 ± 86	<d. l.	75 ± 8		
Yb	9800 ± 3989	250 ± 54	1310	174 ± 40		
Lu	8515 ± 5041	<d. l.	960	<d. l.		
Hf	298 ± 81	155 ± 61	<d. l.	<d. l.		
n[¥]	4	15	1	10		
Data obtained by LA-ICP-MS						
	[¥]		[¥]		[¥]	
La	71 ± 16		101 ± 31		53 ± 18	213 ± 71
Ce	471 ± 53		300 ± 46		49 ± 8	195 ± 33
Pr	240 ± 21		165 ± 22		31 ± 8	122 ± 32
Nd	297 ± 33		205 ± 31		37 ± 14	147 ± 54
Sm	322 ± 50		271 ± 45		41 ± 14	165 ± 56
Eu	328 ± 56		306 ± 48		312 ± 65	1249 ± 260
Gd	262 ± 47		263 ± 45		25 ± 6	102 ± 23
Tb	254 ± 52		282 ± 50		16 ± 4	63 ± 15
Dy	234 ± 52		291 ± 54		6 ± 1	25 ± 5
Ho	228 ± 56		296 ± 59		3 ± 1	13 ± 3
Er	205 ± 53		284 ± 59		4 ± 2	16 ± 6
Tm	202 ± 55		290 ± 65		2 ± 0.3	6 ± 1
Yb	223 ± 61		331 ± 78		2 ± 1	9 ± 4
Lu	204 ± 56		312 ± 73		1 ± 0.3	5 ± 1
Hf	268 ± 47		130 ± 28		11 ± 2	43 ± 7
n[¥]	24		28		9	9

Note: [#], Calculated from the concentrations in the diamond aggregate (see text for explanation); [¥], Results are the average of *n* measurements, errors are calculated as $\sigma/\sqrt{n}$.
<d. l., below detection limit (La = 55 ppm, Nd = 45 ppm, Yb and Hf = 100 ppm, Lu = 260 ppm).

Sodium can be used to derive concentration in the fluid from the analyses made in the diamond aggregate assuming that (1) all the Na incorporated as NaCl in the system resided in the fluid phase at H*P*-H*T* (*i.e.*, no Na in garnet, Table 4) and that no Na is lost in the course of the late evaporation process.

Mass balance for any chemical species *j* requires that

$$m_j^{\mathrm{flH}P} = m_j^{\mathrm{diam}} \tag{1}$$

where m_j^i is the mass of element *j* in phase *i* (either fluid, flH*P*, or diamond aggregate, diam).

Equation (1) can be rewritten as

$$C_j^{\mathrm{flH}P} M_{\mathrm{flH}P} = C_j^{\mathrm{diam}} M_{\mathrm{diam}} \tag{2a}$$

or

$$\frac{C_j^{\mathrm{fHPl}}}{C_j^{\mathrm{diam}}} = \frac{M_{\mathrm{diam}}}{M_{\mathrm{flH}P}} \tag{2b}$$

where C_j^i is the concentration of element *j* in phase *i* and M_i is the mass of phase *i*.

In particular, this equation writes for Na as

$$\frac{C_{\mathrm{Na}}^{\mathrm{flH}P}}{C_{\mathrm{Na}}^{\mathrm{diam}}} = \frac{M_{\mathrm{diam}}}{M_{\mathrm{flH}P}} \tag{3}$$

and from Equations (2b) and (3), we get

$$\frac{C_j^{\mathrm{flH}P}}{C_j^{\mathrm{diam}}} = \frac{C_{\mathrm{Na}}^{\mathrm{flH}P}}{C_{\mathrm{Na}}^{\mathrm{diam}}} \tag{4}$$

Assuming that the sodium concentration in the fluid is the same at high pressure as in the initial solution (*i.e.,* Na is entirely retained into the fluid phase and the fluid mass remains unchanged), we finally get for any chemical species *j*

$$C_j^{\mathrm{flH}P} = C_j^{\mathrm{diam}} \frac{C_{\mathrm{Na}}^0}{C_{\mathrm{Na}}^{\mathrm{diam}}} \quad (5)$$

where C_{Na}^0 is the concentration of Na in the initial solution.

We define here a factor *K* as

$$K = \frac{C_{\mathrm{Na}}^0}{C_{\mathrm{Na}}^{\mathrm{diam}}} = \frac{M_{\mathrm{diam}}}{M_{\mathrm{flH}P}} \quad (6)$$

Using $Na_2O = 1.61$ wt% in diamonds and an initial NaCl-content of 96 $g.l^{-1}$ in the starting solution, a value of 4.01 is estimated for *K*. Concentrations of REE and Hf in the H*P*-fluid are calculated using this value of K and relation (5).

3.4. Mass balance

Mass balance data reported in Table 5 are calculated according to the equation:

$$m_j^0 = m_j^{\mathrm{PyrS2}} + m_j^{\mathrm{flH}P},$$

where

m_j^0 is total mass of element introduced in the experiment via both S1 and S2,

m_j^{PyrS2} is the mass of element *j* borne by pyrope in Step 2 and

$m_j^{\mathrm{flH}P}$ is the mass of element *j* borne by the H*P* fluid in Step 2.

Due to the two-steps experiment strategy and assuming that all the trace elements are borne by pyrope in S1,

$$m_j^0 = m_j^{\mathrm{fluidS2}} + \frac{m_{\mathrm{Pyr}}^{\mathrm{S2}}}{m_{\mathrm{Pyr}}^{\mathrm{S1}}} \times m_j^{\mathrm{fluidS1}},$$

where

m_j^{fluidS1} and m_j^{fluidS2} are the mass of element *j* initially borne by the fluid, respectively in Step 1 and Step 2,

$m_{\mathrm{Pyr}}^{\mathrm{S1}}$ and $m_{\mathrm{Pyr}}^{\mathrm{S2}}$ are the masses of pyrope used for respectively Step 1 and Step 2.

If concentrations in garnets and fluids are properly retrieved, then the total mass must equal the initial mass m_j^0

It appears that most of the trace elements are located in garnet (from *ca.* 70 to 100 % of the initial mass, Table 5). The ratio between the mass of trace elements contained in the fluid and the initial mass ranges from less than 1 to 19 ± 6% depending on the considered element. As expected if no additional REE- and Hf-bearing phase is present in significant amount, the total mass calculated from the concentrations measured in garnet and in the diamond aggregate approximately equals the initial mass (within error). Remarkably high deviation is encountered for La (only 60 ± 20% retrieved from mass balance calculation) and Eu (232 ± 44%). The likely reason for lanthanum deficit is the occurrence of La in a phase which was not taken into account in the mass balance calculation. (La)-törnebohmite was identified in S1 and has partly survived in S2 (Fig. 3). About 4.5 µg of La is missing in the mass balance and could be hosted by residual törnebohmite which would then represent *ca.* 200 ppm of the solid charge. The good agreement between La concentration derived by EMP data on garnet devoid of törnebohmite inclusions and La concentration retrieved from ICP-MS shows that the latter are not affected by the contribution of törnebohmite inclusions. The case of europium is different since (1) no significant Eu has been analyzed in törnebohmite (Table 3), (2) the total Eu calculated by mass balance (28.21 ± 5.13 µg) is more than twice the total Eu effectively introduced in the system (12.16 ± 0.06 µg). The Eu

Table 5. Mass balance calculation for trace elements in S2. See text for calculation details.

	Total mass m_j^0 (µg)	m_j^{Pyr} (µg)	$m_j^{\mathrm{Pyr}} / m_j^0$	$m_j^{\mathrm{flH}P}$ (µg)	$m_j^{\mathrm{flH}P} / m_j^0$	$\frac{m_j^{\mathrm{Pyr}} + m_j^{\mathrm{flH}P}}{m_j^0}$
S2						
La	11.99 ± 0.06	4.97 ± 1.47	0.41 ± 0.12	2.32 ± 0,77	0.193 ± 0.064	60 ± 20
Ce	12.16 ± 0.06	12.87 ± 2.21	1.06 ± 0.18	2.12 ± 0,36	0.175 ± 0.029	135 ± 27
Pr	12.90 ± 0.06	7.78 ± 1.06	0.60 ± 0.08	1.33 ± 0,35	0.103 ± 0.027	71 ± 14
Nd	12.36 ± 0.06	9.56 ± 1.47	0.77 ± 0.12	1.60 ± 0,59	0.129 ± 0.048	92 ± 20
Sm	12.13 ± 0.06	12.03 ± 2.15	0.99 ± 0.18	1.80 ± 0,61	0.148 ± 0.051	121 ± 27
Eu	12.16 ± 0.06	13.20 ± 2.29	1.08 ± 0.19	13.62 ± 2,84	1.119 ± 0.233	232 ± 44
Gd	12.44 ± 0.06	10.90 ± 2.16	0.88 ± 0.17	1.11 ± 0,25	0.089 ± 0.020	110 ± 27
Tb	12.46 ± 0.06	10.98 ± 2.40	0.88 ± 0.19	0.69 ± 0,16	0.055 ± 0.013	114 ± 30
Dy	12.28 ± 0.06	10.77 ± 2.60	0.88 ± 0.21	0.28 ± 0,06	0.022 ± 0.005	115 ± 32
Ho	12.57 ± 0.06	10.52 ± 2.81	0.84 ± 0.22	0.14 ± 0,03	0.011 ± 0.003	113 ± 35
Er	11.95 ± 0.06	9.85 ± 2.83	0.82 ± 0.24	0.17 ± 0,07	0.014 ± 0.006	115 ± 34
Tm	12.68 ± 0.06	9.66 ± 3.11	0.76 ± 0.25	0.07 ± 0,01	0.005 ± 0.001	110 ± 39
Yb	12.90 ± 0.06	10.74 ± 3.73	0.83 ± 0.29	0.10 ± 0,04	0.007 ± 0.003	123 ± 48
Lu	13.66 ± 0.06	10.12 ± 3.49	0.74 ± 0.26	0.05 ± 0,01	0.004 ± 0.001	109 ± 48
Hf	7.05 ± 0.04	6.14 ± 1.35	0.87 ± 0.19	0.46 ± 0,08	0.066 ± 0.011	95 ± 10

content in garnet is similar to the concentration of Sm and Gd, the two neighbor REE (Table 4) excluding therefore an analytical artifact in the determination of the Eu concentration in garnet. By contrast, the Eu concentration in the diamond aggregate is more than 10 times the corresponding Sm and Gd concentrations. Crystallization at H*P*-H*T* of Eu-bearing phase(s) in the pores of the diamond aggregate is therefore the most likely reason for such deviation from mass balance, but such phase(s) remain to be identify. This artifact precludes to the derivation of a meaningful partition coefficient between garnet and aqueous fluid for Eu.

3.5. Partition coefficients

Partition coefficient D_j of trace element j between aqueous fluid with NaCl and pure pyrope is defined by the ratio $C_j^{\mathrm{flH}P} \Big/ C_j^{\mathrm{Pyr}}$ where $C_j^{\mathrm{flH}P}$ represents the concentration of the element j in the high pressure fluid flH*P* as calculated before and C_j^{Pyr} represents the concentration of element j in pyrope Pyr from Step 2 (Table 6).

The value obtained for D_{La} is 2.10 ± 0.95 which indicates that La is more compatible in the NaCl fluid than in the pyrope. For the other LREE (from Ce to Sm), D is lower than 1 ($D_{Ce} = 0.65 \pm 0.15$, $D_{Pr} = 0.74 \pm 0.22$, $D_{Nd} = 0.71 \pm 0.29$ and $D_{Sm} = 0.61 \pm 0.23$). Europium partitioning is not calculated since it does not comply with mass balance. D_{MREE} (Gd and Tb) equals 0.39 ± 0.11 and 0.22 ± 0.07 respectively. D_{HREE} (Dy to Lu) ranges from 0.09 ± 0.02 to 0.02 ± 0.01 with a regular decrease from Dy to Lu. D_{Hf} is 0.33 ± 0.09. The Hf fluid/pyrope partition coefficient (D_{Hf} = 0.33 ± 0.09) indicates that this element favourably partition into garnet.

The pyrope/fluid partition coefficients were plotted (Fig. 6) as a function of the REE^{3+} effective ionic radius (VIII coordination number) taken from Shannon (1976). Partition coefficients for HREE and MREE could be successfully modeled by a charge- and radius-control model (CHARAC model) using the parameters derived by Van Westrenen *et al.* (2003) for pyrope (*i.e.*, r_0 = 0,938 Å and E_x = 748 GPa) with D_0 = 105 (Fig. 6). Eu was also plotted although its $D^{pyr/fluid}$ is meaningless. As already shown by Stalder *et al*. (1998) for pyrope at 5 GPa and 1000 °C, LREE are found to significantly departs from this model which assumes that partition coefficients are only controlled by the crystal-chemistry of the host mineral, here pyrope. Several reasons could be invoked to account for this apparent discrepancy: increasing non-CHARAC behavior when REE-radius deviates from r_0 (Stalder *et al*., 1998), high REE concentration in the experimental system (500 ppm), *i.e.* beyond the limits of Henry's law behavior (Brenan *et al*., 1995) or analytical artifact due to the contamination of the LREE analyses in garnet by residual törnebohmite or trapped fluid. For lanthanum, microprobe data indicate pyrope rims with [La] = 120 ± 5 ppm close to the LA-ICPMS data ([La] = 101 ± 30 ppm) taken to derive partition coefficients. If the garnet rims are considered to reflect equilibrium composition with the H*P*-H*T* fluid trapped in the diamond aggregate in S2 then the contamination assumption does not hold.

4. Discussion

4.1. Two-step experiment

Almost all the garnets crystallized during Step 1 have a HREE-enriched core, whereas pyropes crystallized during the second step from the powder resulting from the first step zoned garnet do not display such zoning, as shown by both SEM observations (Fig. 3) and EMP analysis. In the rare case of zoning Yb (and Lu) content in the core is about 10 times lower than those of Step 1. The average concentrations measured from LA-ICP-MS analysis (Fig. 7) are almost similar in both runs (particularly for MREE and HREE), what is probably linked to the fact that the diameter of laser spot is close to the pyrope diameter. One laser shot therefore samples the whole grain in both runs, except maybe the outer shell (this may account for relatively low La concentrations that are retrieved by ICP-MS, Table 5). This two-step strategy shows that 6 days (Step 2 run duration) are sufficient to approach equilibrium as indicated by the relaxation of chemical heterogeneities inherited from Step 1. In addition, this strategy applied to a simple system (pyrope + water) allowed us to rule out the Eu partition coefficient between fluid and garnet on a mass balance basis.

4.2. Trace element content in the H*P*-H*T* fluid and partition coefficient with garnet: implications

Data obtained on pyrope end-member (and composition along the pyrope-grossular join) equilibrated at 5 GPa, 1000 °C with pure water (Stalder *et al*., 1998) compare very well with the data that we obtained from S2 (Fig. 8) although the bulk trace element content differed by *ca.* one order of magnitude between the two studies. The

Table 6. Partition coefficients between high pressure fluid and pyrope ($D^{\mathrm{flH}P/\mathrm{Pyr}}$) at 850 °C and 3 GPa.

	La	Ce	Pr	Nd	Sm	Eu	Gd	Tb	Dy	Ho	Er	Tm	Yb	Lu	Hf
$D^{\mathrm{NaClfluid}/\mathrm{Pyr}}$	2.10	0.65	0.74	0.71	0.61	4.09	0.39	0.22	0.09	0.04	0.05	0.02	0.03	0.02	0.33
±	0.95	0.15	0.22	0.29	0.23	1.07	0.11	0.07	0.02	0.01	0.02	0.01	0.01	0.01	0.09

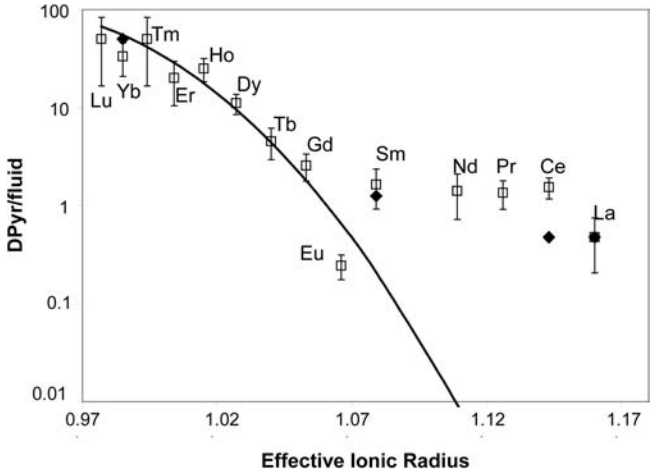

Fig. 6. Partition coefficients ($D^{Pyr/fluid}$) plotted as a function of effective ionic radius. Empty squares: pyrope, NaCl solution, 850 °C, 3 GPa (this study). Plain diamonds: pyrope, pure water, 1000 °C, 5 GPa (Stalder *et al*., 1998). Curve: CHARAC model using the parameter recommended for pyrope by van Westrenen *et al*. (2003) at 850 °C with $D_0 = 105$.

incompatibility of La in pyrope garnet is confirmed here for NaCl-bearing solution. Partition coefficients for middle to heavy REE (and Hf) between garnet ($Alm_{33}Py_{33}Gr_{33}$) and pure water by Kessel *et al*. (2005) obtained at 4 GPa (700 and 800 °C) show the same trend but with values about one order of magnitude lower than those of Stalder *et al.* (1998) and ours. This could be related to differences in garnet composition ($Alm_{33}Py_{33}Gr_{33}$ *vs.* pure pyrope). Interestingly, the ''decoupling'' between Lu (or Yb) and Hf is roughly the same in all three studies, *i.e.* about one order of magnitude.

4.3. Major elements and Eu anomalous concentrations in the diamond aggregate

Electron microprobe data collected on the diamond aggregate indicate unexpectedly high Al_2O_3 and SiO_2 concentration of around 8 and 4.5 wt%, respectively (Table 4). These values can be converted into concentration in the H*P*-H*T* fluid which then reaches unrealistic high concentrations of 33 and 16–19 wt%, respectively. Even if it can be argued that the presence of silica significantly increases the solubility of Al_2O_3 in aqueous system (Tropper & Manning, 2005; Newton & Manning, 2010) through complexing between Al and Si, Al concentration of the order of 13 millimolal only was found in an aqueous solution saturated with respect to both quartz and corundum at 800 °C and 1 GPa (Manning, 2006). Therefore concentrations of the order of less than 0.1 wt% Al_2O_3 would be expected. In addition, the fact that Al concentration in the product precipitated in the diamond aggregate exceeds that of Si is another anomaly. It is interesting to note that the molar ratio between Al_2O_3 and SiO_2 in the diamond aggregate is close to 1.0, therefore the stoichiometry of the corresponding solid products approaches that of Al_2SiO_5. Following Verlaguet *et al*. (2006), the unexpected high Al and Si concentration in the diamond aggregate can

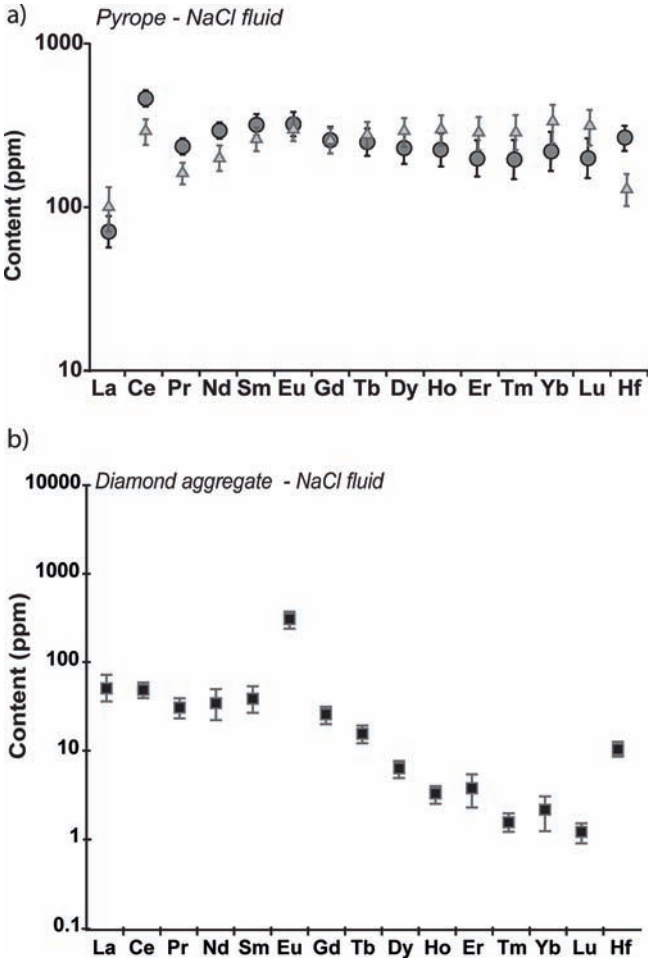

Fig. 7. Diagram displaying average values of trace elements concentrations in ppm in pyrope from both Step 1 and Step 2 and in diamond aggregates. (a) in pyrope (*circles*: Step 1 and *triangles*: Step 2), (b) in diamond aggregate (Step 2 only).

be interpreted as resulting from the incongruent dissolution of the garnet starting material by the solution at high pressure and temperature. Europium displays the same behavior as major elements; it is enriched in the aggregate according to a process which does not only involve quenching of the H*P*-H*T* fluid. The Eu-bearing product in the diamond aggregate has not been identified. The origin of this distinct behaviour for Eu in comparison to the other trace elements remains unclear. A tentative explanation would be the distinctive Eu ability to turn divalent. For example, the formation of an $EuCl_4^{2-}$ aqueous complex has already been described at lower pressure and temperature (400 °C and 500 bars, Allen & Seyfried, 2005). Formation of such complex could change Eu mobility in aqueous solution and favor mass transfer from the sample powder to the diamond trap.

Thermal gradient along the experimental charge is another potential source of mass transfer (*e.g.*, Goffé *et al*., 1987). Matter is then expected to precipitate in the coldest region. The sample was positioned in the ''isothermal'' region of the pressure cell and, owing to the temperature distribution in that region (Schilling & Wunder, 2004), it is very unlikely that the sample center (diamond aggregate)

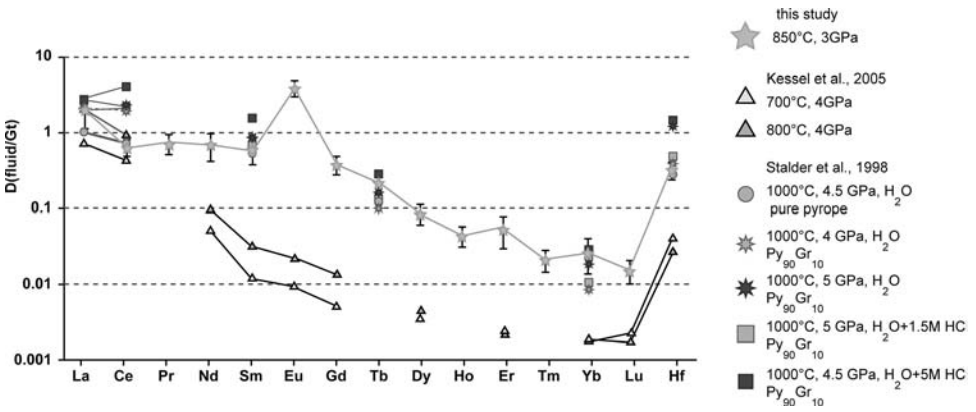

Fig. 8. Comparison of partition coefficients obtained with NaCl fluid (this study, □) and of those obtained in previous studies (Stalder *et al*., 1998; Kessel *et al*., 2005).

represents the coldest region. Furthermore, the fact that Al had been more efficiently transported with respect to Si does not support the thermal gradient assumption.

5. Summary and conclusions

- Two-step experiment strategy significantly decreases the heterogeneities of crystallized minerals and shows that a run duration of about 6 days at 850 °C and 3 GPa, is sufficient to approach chemical equilibrium in garnet (chemical heterogeneity relaxation).
- The use of a single mineral phase (pyrope) allowed a mass balance calculation that led to the exclusion of Eu from the partition coefficient dataset.
- Partition coefficients of REE between fluid and pyrope, at 850 °C, 3 GPa, broadly decrease from LREE toward HREE. The $D^{flH\mathit{P}/Pyr}$ partition coefficients for HREE and MREE are lower than 1 in a NaCl-bearing solution. The partition coefficients for LREE are close to 1 but could be much higher if a CHARAC behavior is assumed.
- The addition of NaCl into water does not significantly affect partition coefficients of REE and Hf, compared to pure water.
- Eu displays a mobility behavior at H*P*-H*T* which contrasts with that of the other trace elements studied here. Formation of Eu-chloride aqueous complexes, as already reported from the literature, could be the reason.

Acknowledgements: The authors acknowledge Nathaniel Findling for XRD analyses, Rémi Freydier and Frédéric Candaudap for LA-ICP-MS analyses, Delphine Yeghicheyan, Jérôme Marin and Luc Marin for their help in chemical analysis. CM is grateful to François Faure and Laurent Tissandier for their help and their advice in sample preparation. We appreciated the thoughtful reviews by Craig Manning and Peter Ulmer, which tremendously improved the manuscript. This work benefited from INSU-CNRS funding (3F program).

References

Allen, D.E. & Seyfried, W.E. (2005): REE controls in ultramafic hosted MOR hydrothermal systems: an experimental study at elevated temperature and pressure. *Geochim. Cosmochim. Acta*., **69**, 675–683.

Ayers, J.C., Dittmer, S.K., Layne, G.D. (1997): Partitioning of elements between peridotite and H_2O at 2.0–3.0 GPa and 900–1100 °C, and application to models of subduction zone processes. *Earth Planet. Sci. Lett.*, **150**, 381–398.

Bau, M. (1996): Controls on the fractionation of isovalent trace elements in magmatic and aqueous systems: evidence from Y/Ho, Zr/Hf and lanthanide tetrad effect. *Contrib. Mineral. Petrol.*, **123**, 323–333.

Becker, H., Jochum, K.P., Carlson, R.W. (2000): Trace element fractionation during dehydration of eclogites from high-pressure terranes and the implications for element fluxes in subduction zones. *Chemical Geol.*, **163**, 65–69.

Brenan, J.M. (1993): Partitioning of fluorine and chlorine between apatite and aqueous fluids at high pressure and temperature: implications for F and Cl content of high *P-T* fluids. *Earth Planet. Sci. Lett.*, **117**, 251–263.

Brenan, J.M., Shaw, H.F., Phinney, D.L., Ryerson, F.J. (1994): Rutile-aqueous fluid partitioning of Nb, Ta, Hf, Zr, U and Th: implications for high field strength element depletions in island-arc basalts. *Earth Planet. Sci. Lett*, **128**, 327–339.

Brenan, J.M., Shaw, H.F., Ryerson, F.J., Phinney, D.L. (1995): Mineral-aqueous fluid partitioning of trace elements at 900°C and 2.0 GPa: Constraints on the trace element chemistry of mantle and deep crustal fluids. *Geochim. Cosmochim. Acta*, **59**, 3331–3350.

Brunet, F. & Chazot, G. (2001): Partitioning of phosphorus between olivine, clinopyroxene and silicate glass in a spinel lherzolite xenolith from Yemen. *Chemical Geol.*, **176**, 51–72.

Duchêne, S., Blichert-Toft, J., Luais, B., Télouk, P., Lardeaux, J.M., Albarède, F. (1997): The Lu-Hf dating garnets and the ages of the Alpine high-pressure metamorphism. *Nature*, **387**, 586–589.

Elliot, T. (2003): Tracers of the slab. *Geophysical Monograph*, **138**, 23–45.

Elliot, T., Plank, T., Morris, J., Zindler, A. (1997): Timescales and element transport in the subduction zone: the Mariana arc as a representative case study. in Abstract of rates and timescales of magmatic processes (ed. Geol. Soc. London).

Feineman, M.D., Ryerson, F.J., DePaolo, D.J., Plank, T. (2007): Zoisite-aqueous fluid trace element partitioning with implications for subduction zone fluid composition. *Chemical Geol.*, **239**, 250–265.

Fryer, P., Gill, J.B., Jackson, M.C. (1997): Volcanologic and tectonic evolution of the Kasuga seamounts, northern Mariana Trough: Alvin submersible investigations. *J. Volcanol. Geotherm. Res.*, **79**, 277–311.

Gammons, C.H., Wood, S.A., Williams-Jones, A.E. (1996): The aqueous geochemistry of the rare earth elements and yttrium: VI. Stability of neodymium chloride complexes from 25 to 300°C. *Geochim. Cosmochim. Acta*, **60**, 4615–4630.

Goffé, B., Murphy, W.M., Lagache, M. (1987): Experimental Transport of Si, Al and Mg in Hydrothermal Solutions - an Application to Vein Mineralization During High-Pressure, Low-Temperature Metamorphism in the French Alps. *Contrib. Mineral. Petrol.*, **97**, 438–450.

Haas, J.R., Shock, E.L., Sassani, D.C. (1995): Rare-Earth Elements in Hydrothermal Systems - Estimates of Standard Partial Molal Thermodynamic Properties of Aqueous Complexes of the Rare-Earth Elements at High-Pressures and Temperatures. *Geochim. Cosmochim. Acta*, **59**, 4329–4350.

Harrison, W.J., Wood, B.J. (1980): An experimental investigation of the partitioning of REE between garnet and liquid with reference to the role of defect equilibria. *Contrib. Mineral. Petrol.*, **72**, 145–155.

Hollister, L.S. (1966): Garnet zoning: An interpretation based on the Rayleigh fractionation model. *Science*, **154**, 1647–1651.

Hulme, S.M., Wheat, C.G., Fryer, P., Mottl, M.J. (2010): Pore water chemistry of the Mariana serpentinite mud volcanoes: a window to the seismogenic zone. *Geochem. Geophys. Geosyst.*, **11**, Q01X09.

Keppler, H. (1996): Constraints from partitioning experiments on the composition of subduction-zone fluids. *Nature*, **380**, 237–240.

Kessel, R., Schmidt, M.W., Ulmer, P., Pettke, T. (2005): Trace element signature of subduction-zone fluids, melts and supercritical liquids at 120 - 180 km depth. *Nature*, **437**, 724–727.

Klinkhammer, G.P., Elderfield, H., Edmond, J.M., Mitra, A. (1994): Geochemical implications of rare earth element patterns in hydrothermal fluids from mid- ocean ridges. *Geochim. Cosmochim. Acta*, **58**, 5105–5113.

Manning, C.E. (2004): The chemistry of subduction-zone fluids. *Earth Planet. Sci. Lett*, **223**, 1–16.

Manning, C.E. (2006): Mobilizing aluminium in crustal and mantle fluids. *J. Geochem. Exploration*, **89**, 251–253.

Manning, C.E. (2007): Solubility of corundum + kyanite in H_2O at 700°C and 10 kbar: evidence for Al-Si complexing at high pressure and temperature. *Geofluids*, **7**, 258–269.

Maury, R.C., Defant, M.J., Joron, J.L. (1992): Metasomatism of the sub-arc mantle inferred from trace elements in Philippine xenoliths. *Nature*, **360**, 661–663.

Michard, A. (1989): Rare earth element systematics in hydrothermal fluids. *Geochim. Cosmochim. Acta*, **53**, 745–750.

Mottl, M.J. (1992): Pore waters from serpentinite seamounts in the Mariana and Izu- Bonin forearcs, Leg 125: evidence for volatiles from the subducting slab. *Proc. Ocean Drill. Program Si. Results*, **125**, 373–385.

Mysen, B.O. (1979): Trace-element partitioning between garnet peridotite minerals and water-rich vapor: experimental data from 5 to 30 kbar. *Am. Mineral.*, **64**, 274–287.

Newton, R.C. & Manning, C.E. (2010): Role of saline fluids in deep-crustal and upper-mantle metasomatism: insights from experimental studies. *Geofluids*, **10**, 58–72.

Philippot, P. & Selverstone, J. (1991): Trace-element-rich brines in eclogitic veins: implications for fluid composition and transport during subduction. *Contrib. Mineral. Petrol.*, **106**, 417–430.

Plank, T. & Langmuir, C.H. (1993): Tracing trace element from sediment input to volcanic output at subduction zones. *Nature*, **362**, 739–742.

Scambelluri, M. & Philippot, P. (2001): Deep fluids in subduction zones. *Lithos*, **55**, 213–227.

Schilling, F. & Wunder, B. (2004): Temperature distribution in piston-cylinder assemblies. *Eur. J. Mineral.*, **16**, 7–14.

Shannon, R.D. (1976): Revised effective ionic radii and systematic studies of interatomic distances in halides and chalcogenides. *Acta Cryst.*, **A32**, 751–767.

Shen, J. & Moore, P.B. (1982): Törnebohmite, $RE_2Al(OH)[SiO_4]_2$: crystal structure and genealogy of RE(III)Si(IV) ↔ Ca(II)P(V) isomorphisms. *Am. Mineral*, **67**, 1021–1028.

Silver, E., Kastner, M., Fisher, A., Morris, J., McIntosh, K., Saffer, D. (2000): Fluid flow paths in the middle America Trench and Costa Rica margin. *Geology*, **28**, 679–682.

Spandler, C. & Hermann, J. (2006): High-pressure veins in eclogite from New Caledonia and their significance for fluid migration in subduction zones. *Lithos*, **89**, 135–153.

Stalder, R., Foley, S.F., Brey, G.P., Horn, I. (1998): Mineral-aqueous fluid partitioning of trace elements at 900–1200°C and 3.0–5.7 GPa: new experimental data for garnet, clinopyroxene, and rutile, and implications for mantle metasomatism. *Geochim. Cosmochim. Acta*, **62**, 1781–1801.

Tatsumi, Y. & Eggins, S.M. (1995): Subduction zone magmatism. Frontiers in earth sciences. Blackwell Science, Massachusetts, **211**, pp. 34–50.

Tropper, P. & Manning, C.E. (2005): Very low solubility of rutile in H2O at high pressure and temperature, and its implications for Ti mobility in subduction zones. *Am. Mineral.*, **90**, 502–505.

Tropper P., Manning, C.E., Harlov, D.E. (2010): Solubility of $CePO_4$ monazite and YPO_4 xenotime in H_2O and H_2O-NaCl at 800 degrees C and 1 GPa: Implications for REE and Y transportation during high-grade metamorphism. *Chem Geol*, **282**, 58–66.

van Sijl, J., Allan, N.L., Davies, G.R., van Westrenen, W. (2009): Molecular modelling of rare earth element complexation in subduction zone fluids. *Geochim. Cosmochim. Acta*, **73**, 3934–3947.

van Westrenen, W., van Orman, J.A., Watson, H., Fei, Y., Watson, E.B. (2003): Assessment of temperature gradients in multianvil assemblies using spinel layer growth kinetics. *Geochem. Geophys. Geosyst.*, **4**, 1036.

Verlaguet, A. & Brunet, F. (2007): Effect of incongruent dissolution on mineral solubility data derived from quench experiments. *Eur. J. Mineral.*, **19**, 783–789.

Verlaguet, A., Brunet, F., Goffé, B., Murphy, W.M. (2006): Experimental study and modeling of fluid reaction paths in the quartz-kyanite +/− muscovite-water system at 0.7 GPa in the 350–550 °C range: Implications for Al selective transfer during metamorphism. *Geochim. Cosmochim. Acta*, **70**, 1772–1788.

You, C.F. & Gieskes, J.M. (2001): Hydrothermal alteration of hemipelagic sediments: experimental evaluation of geochemical processes in shallow subduction zones. *Appl. Geochem.*, **16**, 1055–1066.

Received 15 June 2010
Modified version received 15 April 2011
Accepted 18 May 2011